Coordination Chemistry of Co(II)-Bleomycin: Its Investigation through NMR and Molecular Dynamics[†,‡]

Teresa E. Lehmann,*[,§] Maria Luisa Serrano,[||] and Lawrence Que, Jr.[⊥]

Laboratorio de Análisis Instrumental, Centro de Química, Instituto Venezolano de Investigaciones Científicas (IVIC), Caracas 1090, Venezuela, Department of Chemistry and Center for Metals in Biocatalysis, University of Minnesota, Minneapolis, Minnesota 55455, and Laboratorio de Modelaje Molecular, Facultad de Farmacia, Universidad Central de Venezuela, Caracas 1041-A, Venezuela

Received August 6, 1999; Revised Manuscript Received November 29, 1999

ABSTRACT: Previous studies on the coordination chemistry of Co−bleomycin have suggested the secondary amine in β-aminoalanine, the N5 and N1 nitrogens in the pyrimidine and imidazole rings, respectively, and the amide nitrogen in β-hydroxyhistidine as equatorial ligands to the cobalt ion. The primary amine in β-aminoalanine and the carbamoyl group of the mannose have been proposed alternatively as possible axial ligands. The first coordination sphere of Co(II) in Co(II)BLM has been investigated in the present study through the use of NMR and molecular dynamics calculations. The data collected from the NMR experiments are in agreement with the equatorial ligands previously proposed, and also support the participation of the primary amine as an axial ligand. The paramagnetic shifts of the gulose and mannose protons could suggest the latter as a second axial ligand. This possibility was investigated by way of molecular dynamics, with distance restraints derived from the relaxation times measured through NMR. The molecular dynamics results indicate that the most favorable structure is six-coordinate, with the primary amine and either the carbamoyl oxygen or a solvent molecule occupying the axial sites. The analysis of the structures previously derived for HOO−Co(III)−bleomycin and HOO−Co(III)−pepleomycin led us to propose the six-coordinate structure with only endogenous ligands, as the one held in solution by the Co(II) derivative of bleomycin.

Bleomycins (BLM) (Figure 1) are a family of glycopeptide-derived antibiotics that have the ability to bind and degrade DNA in the presence of some metal ions (Fe^{2+}, Fe^{3+}, Mn^{2+}, Co^{3+}), which is believed to be responsible for their antitumor activity (*1*−*11*). The presence of ferrous ion and molecular oxygen is proposed to be essential for DNA degradation in vivo (*1*, *10*, *12*). Knowledge of the structure of the biologically relevant Fe(II)BLM[1] is vital to further characterize the mechanism of action of the drug as well as to establish the drug−DNA spatial correlations that could explain the antibiotics specificity toward $^{5'}$-GC-$^{3'}$ and $^{5'}$-GT-$^{3'}$ DNA sequences (*13*). To this end, numerous structural studies on various metallo−BLMs (*1*), BLM analogues (*14*−*20*), and other antibiotics structurally related to BLM, such as pepleomycin (*21*) (PEP) and tallysomycin (*22*) (TLM), have been conducted. The results of these studies have led to very important findings about the coordination chemistry of the CO−Fe(II), Zn(II), Mn(II), Co(II), and Co(III) adducts of the drug (*23*−*29*). In previous work, we have structurally characterized the complex Fe(II)BLM through NMR (*30*). Our NMR studies indicate that the primary and secondary amines in β-aminoalanine, the pyrimidine, and the imidazole and the amide nitrogen in β-hydroxyhistidine are coordinated to the iron in this metallobleomycin. The participation of the carbamoyl group in the mannose moiety as a ligand to the Fe center was ruled out for this complex, based on a structural correlation performed between the Fe(II)− and HOO−Co(III)BLM (*31*) derivatives. Even though the protons in both of the sugar residues exhibit paramagnetic behavior in Fe(II)BLM, the NMR data alone are not enough to determine if mannose is part of the first coordination sphere of the metal in this derivative. To further extend the comparison between the iron and cobalt complexes of bleomycin, both involved in DNA degradation, the coordination chemistry of the paramagnetic Co(II)BLM was investigated through NMR and molecular dynamics in the present study. The structural data derived from this investigation are important because: (1) the oxidation of Co(II)BLM by oxygen produces Co(III)BLM and its peroxide form, HOO−Co(III)BLM, which is involved in DNA cleavage after photochemical activation

[†] This work was supported by the Consejo de Desarrollo Científico y Humanístico (CDCH) Grant CDCH0610429698 and NIH Grants GM-33162 and GM-51849.

[‡] The PDB ID code for model I is 1DEY.

* To whom correspondence should be addressed. Telephone: +58-(02)-504-1702. Fax: +58-(02)-504-1309. E-mail: tlehmann@quimica.ivic.ve.

[§] Instituto Venezolano de Investigaciones Científicas (IVIC).

[||] Universidad Central de Venezuela.

[⊥] University of Minnesota.

[1] Abbreviations: ALA, β-aminoalanine; BIT, bithiazole; BLM, bleomycin; COSY, correlated spectroscopy; ESFF, extensible systematic force field; GUL, gulose; HIS, β-hydroxyhistidine; HMQC, heteronuclear multiple quantum correlation; MAN, mannose; NOE, nuclear Overhauser effect; PEP, pepleomycin; PYR, pyrimidinylpropionamide; THR, threonine; TOCSY, totally correlated spectroscopy; VAL, methylvalerate.

10.1021/bi991841p CCC: $19.00
Published on Web 03/16/2000

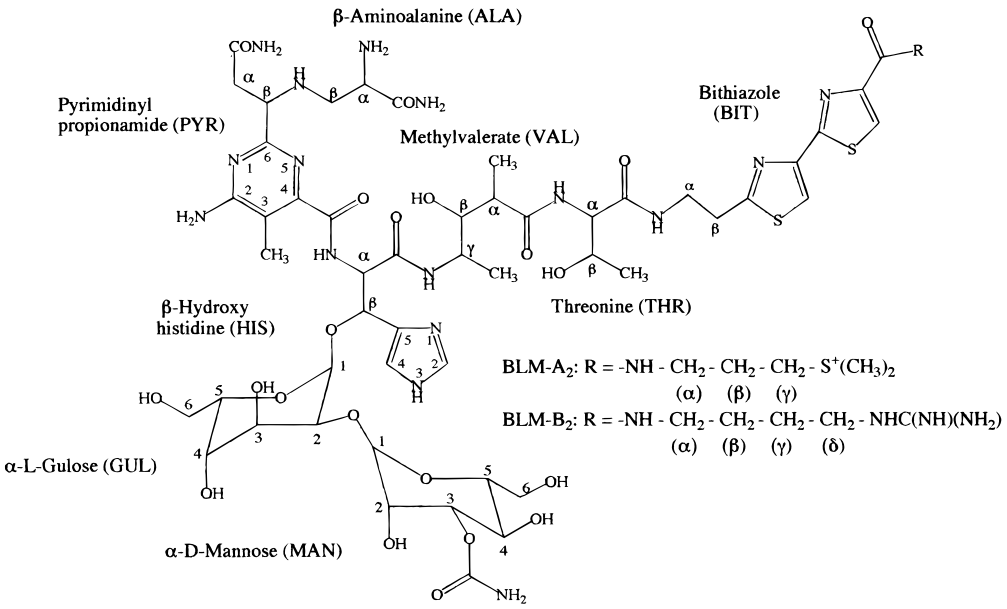

FIGURE 1: Structures of BLM−A_2, and BLM−B_2, the most abundant components of the clinically employed mixture of BLMs.

(*23*, *35*−*40*); (2) a strong analogy between the oxidation chemistry of Co(II)BLM by O_2 and that of Fe(II)BLM has been proposed (*35*, *36*, *40*); (3) when compared with the one observed for Fe(II)BLM, the nuclear line broadening induced by the metal center on the protons close to it in Co(II)BLM is almost two times smaller (*41*). Consequently, the Co(II)BLM ^{1}H NMR signals are sharper and, therefore, easier to ascribe, allowing the validation of the NMR assignments performed earlier for the iron complex of bleomycin (vide infra). Co(II)BLM was investigated by using one- and two-dimensional NMR techniques. Our results indicate that, as in the Fe(II) complex of the antibiotic, the primary and secondary amines in β-aminoalanine, the pyrimidine and imidazole rings, and the amide nitrogen in β-hydroxyhistidine are coordinated to the metal. The protons of the sugar moieties in Co(II)BLM also exhibit paramagnetic behavior. However, their specific assignments are difficult due to the lack of observed NMR connectivities among them, and the similarities between the mannose and gulose spin systems (Figure 1). On the basis of our NMR data, and aiming to define the role of the sugars in the structure of the Co(II)BLM complex, we have modeled its three-dimensional structure through molecular dynamics (MD) calculations. Various coordination alternatives were considered (vide infra). Our MD results favor a six-coordinate model, which includes, besides the coordination sites already identified through NMR, either the carbamoyl oxygen or a solvent molecule as an axial ligand to the Co(II) center. This type of coordination environment was also proposed by Loeb et al. (*42*) for Fe(II)BLM. However, our results allow a more specific location of the BLM residues around the metal center, placing the primary amine and the bithiazole moiety on the same face of the equatorial plane of the metal, with the sugars occupying the opposite face. The analysis of the coordination geometries exhibited by the models favored in the present investigation, in light of the results of previous structural studies performed on some metallo−BLMs that possibly mimic activated BLM, indicates that a six-coordinate solution structure with only endogenous ligands is reasonable for the resting state of CoBLM.

MATERIALS AND METHODS

Co(II)BLM Sample Preparation. Blenoxane, the commercial mixture of bleomycin congeners was a generous gift of Dr. S. L. Lucania, Bristol-Myers Squibb Pharmaceutical Research Institute (Princeton, NJ). It was employed in the experiments without further purification. All samples were prepared under strict oxygen-free conditions. Blenoxane (5 μmol) lyophilized three times from D_2O was dissolved in 0.5 mL of ultrapure D_2O (99.9% D, Cambridge Isotope Laboratories). One equivalent of $Co(NO_3)_2 \cdot 6H_2O$ in D_2O was added to prepare a 10 mM Co(II)BLM sample. The pH (meter reading uncorrected for the deuterium isotope effect) was adjusted to 6.5 with a 50 mM NaOD solution. The sample was transferred to a purged NMR tube, which was immediately sealed. A 1:1 Co(II)/BLM sample in H_2O was prepared by an analogous procedure.

Co(II)BLM NMR. NMR experiments were performed at 300, 360, and 500 MHz on a Varian VXR300, Bruker AMX360, and Varian VXR500 NMR spectrometers, respectively, at room temperature. All chemical shifts were calculated respect to HDO as the internal standard, which was selectively irradiated for 80 ms in all the spectra. The one-dimensional spectra were acquired by using a 90° pulse (10−12 μs in the Varian VXR300 and VXR500, and a 7 μs in the Bruker AMX360) with 13 K data points. An inversion−recovery pulse sequence ($180° - \tau - 90° -$ AQ) was used to obtain nonselective proton longitudinal relaxation times, T_1, with the carrier frequency set at several different positions to ensure the validity of the measurement. Signal-to-noise ratios were improved by using a line-broadening factor of 30 Hz in the Fourier transformation.

COSY spectra covering the paramagnetic region were collected with 800 points in t_2, 400 points in t_1, 280 scans, a spectral width of 36 kHz, and a relaxation delay of 300 ms. In the diamagnetic region, COSY spectra were acquired with 1024 points in t_2, 256 points in t_1, 150 scans, a spectral width of 17 kHz, and a relaxation delay of 1.5 s. COSY spectra of Co(II)BLM in H_2O were acquired with 800 points in t_2, 400 points in t_1, 300 scans, a spectral width of 21 kHz,

and a relaxation delay of 300 ms. A zero-degree-shifted sine bell was applied prior to Fourier transformation, followed by polynomial baseline correction in both dimensions, and symmetrization. The cross-peaks displayed in these spectra were identified prior to symmetrization of the data.

TOCSY spectra of Co(II)BLM in D_2O were collected on the AMX360 NMR spectrometer with 800 points in t_2, 400 points in t_1, 280 scans, a spectral width of 36 kHz, a relaxation delay of 300 ms, and a mixing time of 10 ms. A 60°-shifted sine-squared bell was applied to both dimensions prior to Fourier transformation, followed by polynomial baseline correction in both dimensions. No symmetrization was used in these spectra.

HMQC spectra were acquired with 2048 points in t_2, 128 points in t_1, 80 scans, spectral widths of 17 and 34 kHz, respectively, in the proton and carbon dimensions, and a relaxation delay of 20 ms. In these experiments, the data were weighted with a cosine-squared function prior to Fourier transformation.

Molecular Modeling. All calculations were carried out with Insight II/Discover_3 (Molecular Simulations Inc., Walthman, M. A.) on a Silicon Graphics. Aqueous simulations were carried out using a 10 Å solvent shell. Nonbonded van der Waals interaction was cutoff at 25 Å for the solvent system. The distance-dependent dielectric constant algorithm was used. Molecular dynamics calculations used the Verlet velocity algorithm with a 0.001 ps time step, and scaling every 10 steps. All energy minimizations used the Extensible Systematic Force Field (ESFF) potential. Distance constraints were applied using a flat-bottomed potential. Because of the paramagnetic nature of the Co(II)BLM complex, no NOE or *J*-coupling information was obtained from the NMR experiments, and starting models for the molecular dynamics calculations could not be built. Therefore, the four structures for HOO−Co(III)BLM generated by Wu et al. (*31*) were used as the starting point for the calculations. The metal was changed from Co(III) to Co(II), and the charges and coordination geometries were assigned using the ESFF force field suitable to model systems containing transition metals.

Proton−metal distances were calculated for the paramagnetically behaved protons from their relaxation times using eq 1

$$r_i = r_j\,(T_{1i}/T_{1j})^{1/6} \qquad (1)$$

where r_i and T_{1i} are the proton−metal distance and the relaxation time of proton *i*, respectively. Those distances were used to constraint the involved protons during molecular dynamics calculations.

NOE-like intervals were defined on the basis of the calculation error of the proton−metal distances

$$\Delta r_i = (\partial r_i/\partial r_j)\Delta r_j + (\partial r_i/\partial T_{1i})\Delta T_{1i} + (\partial r_i/\partial T_{1j})\Delta T_{1j} \qquad (2)$$

where Δr_j, ΔT_{1i}, and ΔT_{1j} are the experimental errors on the r_j, T_{1i}, and T_{1j} measurements, respectively. Proton−metal distance-derived constraints were set at $r_j \pm \Delta r_j$, with a force constant of 60 kcal mol^{-1} Å^{-1}.

Five models (vide infra), I−V, of Co(II)BLM with different coordination numbers and geometries were assayed in the molecular dynamics simulated annealing calculations. A 10 Å solvent shell was created around the BLM complex. The water molecules were minimized with the group based cutoff, while holding the BLM complex fixed. Then, the water molecules were fixed, and the BLM complex was minimized with no constraints using the cell multipole method. The BLM structures were first minimized by the steepest descent method, followed by conjugate gradient minimization to a rms gradient of <0.1. The distance constraints were then applied, and the minimization steps were repeated. Molecular dynamics simulated annealing calculations were performed on the minimized structures. The structures were heated and equilibrated over 10 ps from 5 to 1000 K in 10 K increments, with velocities assigned every 0.001 ps. No distance constraints were used in this first step in order to randomize the structures. Molecular dynamics was run for 4 ps, with the distance constraints applied with a force constant of 0.06 kcal mol^{-1} Å^{-1}. Next, the force constants were scaled to 120 kcal mol^{-1} Å^{-1} over 7.6 ps in a series of molecular dynamics runs. The system was allowed to evolve for 6 ps, then cooled to 300 K over 8 ps. At this temperature, the force constants were reduced to their final value of 60 kcal mol^{-1} Å^{-1} over 4 ps in a series of 0.4 ps molecular dynamics runs. The system was allowed to equilibrate for 5 ps, followed by the final 15 ps molecular dynamics run. Ten structures were collected and minimized with constraints after the last dynamics run.

RESULTS AND DISCUSSION

NMR Results. The coordination chemistry of Co(II)BLM was investigated through the use of one- and two-dimensional NMR techniques, such as COSY, TOCSY, and HMQC and molecular modeling. The relaxation times of the protons affected by the paramagnetic influence of the Co(II) center were also measured. The ^{1}H NMR spectrum of Co(II)BLM in D_2O shown in Figure 2A, exhibits 27 paramagnetically shifted resonances. As observed for Fe(II)BLM (*30*), six of these resonances (211, 152, 114, 77.1, −20.5, and −30.5 ppm in Co(II)BLM, Table 1) are very broad (1400−500 Hz) corresponding to protons that are two bonds away from a ligation site (vide infra). All the paramagnetically shifted signals, except the ones at 2.6, −1.9, −3.4, and −4.9 ppm generated by CH_3 groups, are one-proton signals as indicated by integration. When compared with the NMR spectrum of Fe(II)BLM, the spectrum in Figure 2A shows signals two times sharper, with relaxation times that are also longer than their equivalents in Fe(II)BLM. This is as expected for the change of metal center from Fe(II) to Co(II) (*41*). The longer T_1's observed for Co(II)BLM result in more intense cross-peaks in the two-dimensional NMR spectra, which facilitate the assignment of the signals. The excellent HMQC maps have been particularly useful for this study. Unfortunately, saturation transfer (ST) experiments were unsuccessful for Co(II)BLM due to the slower exchange of the Co(II) ion in and out of the BLM molecule (*30*, *33*, *43*), thereby depriving us of another useful assignment tool.

C-Terminal Amine and Bithiazole (BIT) Assignments. The COSY spectrum in Figure 3 shows the signals found in the diamagnetic region for Co(II)BLM. The features for the C-terminal amine in BLM−A2 are located at 3.7 ($C^{\alpha}H_2$), 3.3 ($C^{\gamma}H_2$), and 2.2 ppm ($C^{\beta}H_2$) (Figure 1) and connected through cross-peaks a and b in the COSY spectrum shown in Figure 3. The C-terminal amine in BLM−B2 exhibits signals at 3.5, 3.2, and ∼1.7 ppm. The features at 3.5 and

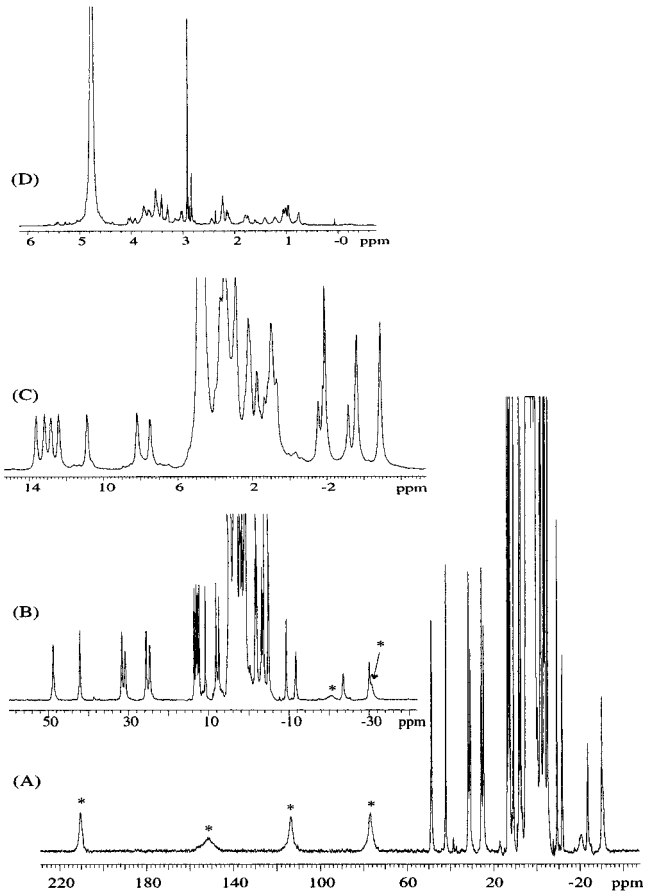

FIGURE 2: (A) ^{1}H NMR spectrum (Varian VXR300 at 299.95 MHz and 298 K) of a 10 mM 1:1 BLM/Co(II) sample in D_2O. (B) and (C) expanded 50−40 ppm and 14−(−4) ppm regions, respectively. (D) Diamagnetic region. Asterisks (*) indicate the six broad signals generated by protons two bonds away from a ligation site.

3.2 ppm are attributed to the $C^{\alpha}H_2$ and $C^{\delta}H_2$ protons (Figure 1), based on the assignment of these signals performed by Chen et al. (*44*) on their NMR study of BLM−A2 and BLM−B2 in aqueous solution. The NMR features for the $C^{\beta}H_2$ and $C^{\gamma}H_2$ protons of this moiety overlap at ∼1.7 ppm. The overlap of these signals was also observed by Chen and co-workers (*44*). The assignments of the features derived from the $(CH_2)_n$ protons of the C-terminal amine in BLM−B2 are supported by the presence of cross-peaks that connect the signals generated by protons $C^{\alpha}H_2$ and $C^{\beta}H_2$, and $C^{\delta}H_2$ and $C^{\gamma}H_2$ (cross-peaks c and d, respectively, in Figure 3). The signals for the BIT α- and *β*-proton (3.4 and 3.1 ppm; cross-peak e) are also found in this region. In the case of Co(II)BLM, the diamagnetic behavior of these protons indicates that they do not participate in metal complexation. The resonances derived from the bithiazole C5 and C5′ ring protons are located in the region between 7.0 and 9.0 ppm (Figure 2B), the same region they occupy in the NMR spectrum of the free form of the antibiotic (*45*).

Threonine (THR) and Valerate (VAL) Assignments. The zone between −0.8 and −6.0 ppm in the NMR spectrum of Co(II)BLM contains the signals for three of the four CH_3 groups present in BLM (Figure 2C, signals at −1.9, −3.4, and −4.9 ppm). These three CH_3 signals are derived from the methyl groups in the THR and VAL segments, as indicated by the COSY connections to one-proton signals observed in the COSY spectra in Figure 4 (cross-peaks a and b), and Figure 5 (cross-peak a). The fourth CH_3 group in BLM, being "isolated" on the pyrimidine ring (*45*), has no two-dimensional connections to nonsolvent−exchangeable signals (Figure 2D).

The methyl signal at −1.9 ppm shows a COSY connection to the feature at 0.8 ppm (Figure 4, cross-peak b), which in turn is connected to the resonance at −1.5 ppm (Figure 4, cross-peak c). This type of connectivity pattern is indicative of a CH−CH(CH_3) spin system. However, the THR and VAL segments both contain such a spin system. The two possibilities can be distinguished by considering the solvent-exchangeable protons in these moieties. As can be seen in Figure 4, the signal at −1.5 ppm exhibits a connection with

Table 1: Summary of the Resonance Positions, Relaxation Times, T_1, and Calculated Proton−Metal Distances for the Protons in Co(II)BLM at pH 6.5

peak position (ppm)				
^{1}H	^{13}C	T_1 (ms)	assignments	H_i−Co distances (Å)
211[a]	[b]	3.7	HIS $C^{\beta}H$	3.9
152[a]	[b]	1.1	1/2 ALA $C^{\beta}H_2$	3.8
114[a]	[b]	3.4	PYR $C^{\beta}H$	3.2
77.1[a]	[b]	3.2	ALA $C^{\alpha}H$	3.8
−20.5[a]	[b]	<1.1	1/2 ALA $C^{\beta}H_2$	<3.2
−30.5[a]	[b]	<1.1	HIS C2H	<3.2
51.8			HIS N3H	
42.1	[b]	17.4	HIS C4H	5.0[c]
31.5	[b]	7.5	HIS $C^{\beta}H$	4.3
24.7	[b]	10.9	1/2 PYR $C^{\alpha}H_2$	4.6
48.8	[b]	12.5	1/2 PYR $C^{\alpha}H_2$	4.7
2.6	20.4	108	PYR CH_3	6.8
15.1			PYR $CONH_2$	
16.2			PYR $CONH_2$	
−4.9	3.0	83.8	VAL $C^{\alpha}CH_3$	6.5
−23.2	[b]	9.4	VAL $C^{\alpha}H$	4.5
−11.8	65.5	20.6	VAL $C^{\beta}H$	5.1
−1.8	35.8	*d*	VAL $C^{\gamma}H$	
−3.4	12.0	51.1	VAL $C^{\gamma}CH_3$	6.0
−1.5	53.0	209	THR $C^{\alpha}H$	7.6
0.8	62.5	277	THR $C^{\beta}H$	7.9
−1.9	15.0	212	THR $C^{\beta}CH_3$	7.6
0.2			THR NH	
26.1	128	18.7	G-1	5.1
12.8	86.2	69.0	G-2	6.3
10.9	82.1	88.4	G-3	6.6
13.7	83.8	107	G-4	6.8
32.0	86.0	18.2	G-5	5.0
12.4	72.0	128	G-6	7.0
13.2	72.0	117	G-6	6.9
4.8	96.2	[e]	M-1	
−9.3	60.0	37.8	M-2	5.7
−29.9	[b]	7.4	M-3	4.3
−3.0	53.8	135	M-4	7.0
2.5	74.1	131	M-5	7.0
2.2	59.1	187	M-6	7.4
3.2	59.1	205	M-6	7.5

[a] The order in which these peaks are listed is not necessarily correlated in a one-to-one fashion to the assignments shown in column 4, since a one-to-one assignment of them could not be reached. [b] Because of the poor relaxation properties of these nuclei, their ^{13}C-NMR signals could not be detected in the HMQC spectra. [c] The proton−metal distance and measured T_1 for the C4H proton in the imidazole ring were the reference values used in eq 1, since the imidazole ring is rigid and, when bound to Co(II), its C4H proton displays typically proton−metal distances of ∼5 Å in models complexes (*57*−*61*). [d] Because of its overlap with the THR $C^{\alpha}H$ and $C^{\beta}CH_3$ protons, the relaxation time of the VAL $C^{\gamma}H$ proton can only be estimated to be between 20.6 and 51.1 ms. [e] The relaxation time for this proton could not be measured due to its strong overlap with the HDO signal.

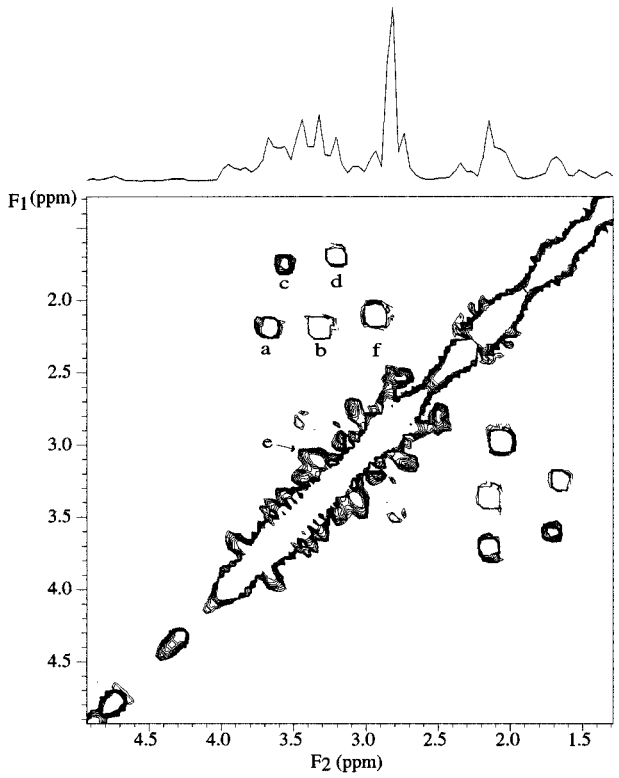

FIGURE 3: ^{1}H COSY spectrum (Varian VXR500 at 499.88 MHz and 298 K) of the 1:1 BLM/Co(II) sample in D_2O covering the diamagnetic region.

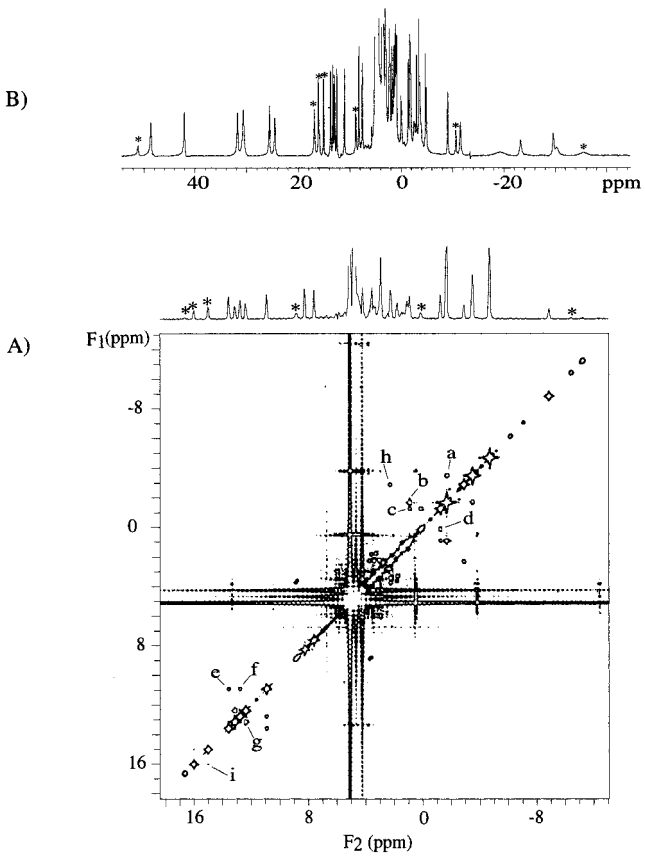

FIGURE 4: (A) ^{1}H COSY spectrum (Varian VXR500 at 499.88 MHz and 298 K) of the 1:1 BLM/Co(II) sample in H_2O. (B) Full one-dimensional spectrum of the same sample. Asterisks (*) indicate the signals generated by H_2O exchangeable NH protons.

a proton-exchangeable resonance located at 0.2 ppm (cross-peak d). This NH−CH−CH(CH_3) connectivity pattern can only be associated with the THR moiety, since this pattern is incompatible with the C$^\alpha$H−C$^\beta$H(CH_3), and C$^\gamma$H(CH_3) spin systems found in the VAL residue. The solvent-exchangeable signal must then arise from the NH group on the peptide bond between the VAL and THR moieties. The signal arising from this solvent-exchangeable proton was also found to be correlated to the THR C$^\alpha$H proton for Fe(II)-BLM (*30*). The assignment of the CH−CH(CH_3) spin system just discussed to the THR moiety is also corroborated by the ^{13}C NMR chemical shifts of the carbons in this spin system determined from the HMQC spectrum shown in Figure 6. The ^{13}C NMR positions for the C$^\alpha$H, C$^\beta$H, and C$^\beta CH_3$ carbons in the THR residue are located, at 60.2, 68.1, and 20.0 ppm, respectively, in the Zn(II) adduct of BLM, as reported by Williamson et al. (*46*). For Co(II)BLM, these carbons are positioned at 53.0, 62.5, and 15.0 ppm, respectively (cross-peaks a−c). The difference between the Zn(II)BLM and Co(II)BLM THR carbons probably reflects the influence of the paramagnetic center on the latter. Even though the ^{13}C chemical shifts of the THR carbons do not exactly coincide in both adducts, their relative positions, as well as the locations of all the other ^{13}C NMR signals in Figure 6, showing concordance with their respective partners in Zn(II)BLM (*46*) (vide infra), are evidence in favor of the THR NMR assignments just made.

With the THR spin system identified, the CH_3 signals at −4.9 and −3.4 ppm can be attributed to the methyl groups in the VAL segment. The CH_3 signal at −4.9 ppm is correlated with a single-proton feature at −23.2 ppm (Figure 5A, cross-peak a), while the CH_3 signal at −3.4 ppm is correlated to the single-proton resonance at −1.8 ppm (Figure 4A, cross-peak a), which is in turn connected to another single-proton feature at −11.8 ppm (Figure 5A, cross-peak b). As can be seen from the spectra in Figures 4 and 5A, the VAL segment does not show a full network of connections; there are two sets of correlated signals containing the CH(CH_3) and CH−CH(CH_3) subsystems. These two spin subsystems are similarly unconnected in the NMR spectrum of Fe(II)BLM, which has been attributed to the small coupling constant between the VAL C$^\alpha$H and C$^\beta$H protons (*30*, *31*). By analogy to the assignments for Fe(II)BLM, the signals at −23.2 and −4.9 ppm are assigned to the VAL C$^\alpha$H and C$^\alpha CH_3$ protons, respectively, and the remaining correlated signals for this moiety are attributed to the CH−CH(CH_3) set of protons. As in Fe(II)BLM (*30*), the C$^\alpha$H proton is the most shifted of the protons in the VAL segment and has the shortest T_1, consistent with its proximity to the metal center. The remaining protons exhibit HMQC connections to ^{13}C features that corroborate the signal assignments. For example, the VAL C$^\beta$ and C$^\gamma$ carbons are assigned to the signals at 65.5 and 35.8 ppm (Figure 6, cross-peaks r and f, respectively). These relative ^{13}C chemical shifts are, as expected, given the attachment of the VAL C$^\beta$ and C$^\gamma$ carbons to an OH and a NH groups, respectively (Figure 1). The same trend regarding the ^{13}C chemical shifts of the VAL C$^\beta$ and C$^\gamma$ carbons is observed for Zn(II)BLM (75.4 and 48.6 ppm for the C$^\beta$ and C$^\gamma$ carbons, respectively (*46*)). The positions of the C$^\alpha$(CH_3) and C$^\gamma$(CH_3) methyl carbons in the HMQC spectrum in Figure 6 (cross-signals d and e) are also compatible with the location of the ^{13}C NMR signals in

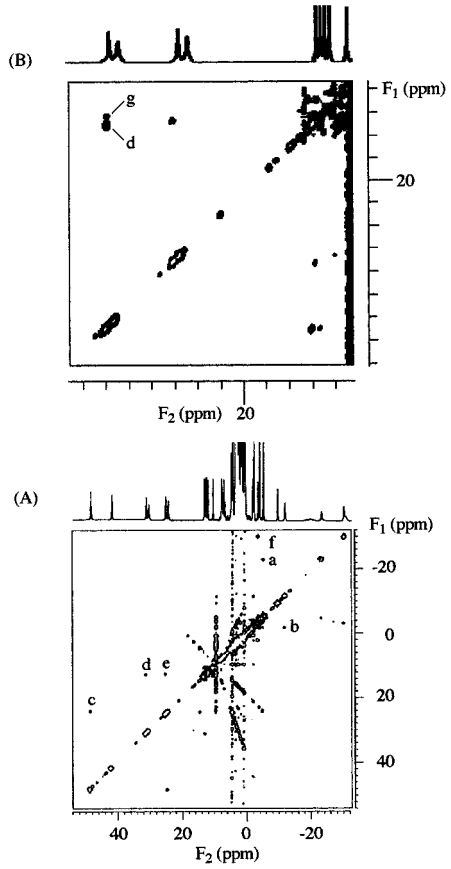

FIGURE 5: COSY (A) and TOCSY (B) spectra (Bruker AMX360 at 360.13 MHz and 298 K) of the 1:1 BLM/Co(II) sample in D_2O.

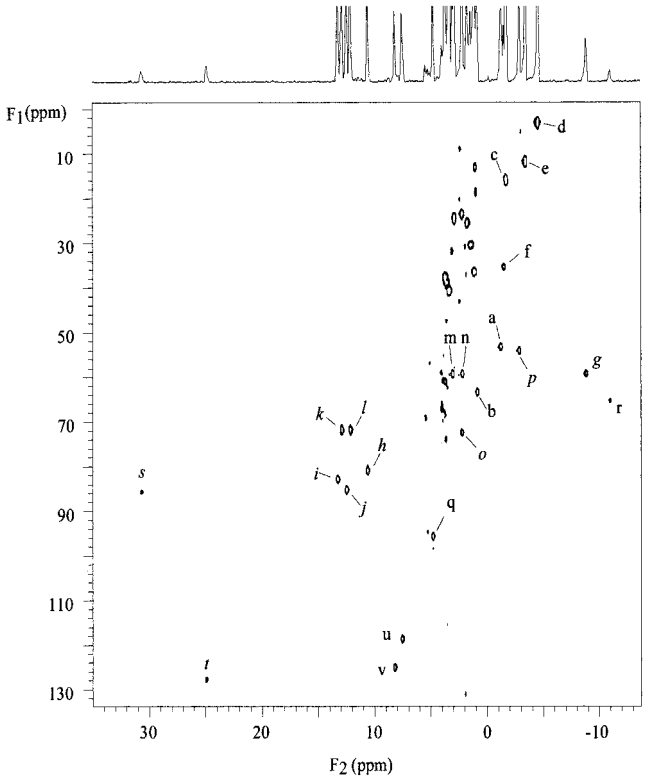

FIGURE 6: HMQC spectrum (VXR500 at 499.88 MHz and 298 K) of the 1:1 BLM/Co(II) sample in D_2O, showing the ^{13}C NMR signals exhibited by some of the carbon atoms in the THR, VAL, MAN (italics), and GUL (roman) fragments.

Zn(II)BLM. These carbons have chemical shifts of 3.0 and 12.0 ppm in Co(II)BLM, and 13.1 and 15.8 in Zn(II)BLM, respectively. We have thus fully identified the NMR signals arising from the THR and VAL fragments in Co(II)BLM.

Gulose (GUL) and Mannose (MAN) Assignments. The sugar protons in the BLM molecule can in principle be identified via their extensive spin systems, as revealed by COSY and/or TOCSY connections. As in the Fe(II)BLM case, four networks of signals can be identified that can only be associated with the sugar protons. The longer relaxation times exhibited by the protons in Co(II)BLM relative to the Fe(II) adduct result in more intense cross-peaks in the two-dimensional maps, which facilitate the assignments of these signals.

The first network of signals involves three protons. The TOCSY spectrum in Figure 5B shows the signal at 32.0 ppm connected to the features at 13.2 and 12.4 ppm (cross-peaks d and g). The two latter resonances are in turn connected to each other via a COSY cross-peak (Figure 4, cross-peak g) and correlated to the same carbon atom as shown in the HMQC spectrum in Figure 6 (cross-signals k and l). This set of correlations provides evidence for the presence of a $CH-CH_2$ spin subsystem. Being part of one of the two sugar moieties, this spin subsystem can only be associated with the $C5H-C6H_2$ portion.

The second set of connected signals includes the feature at 26.1 ppm connected, via a COSY cross-peak, to the one at 12.8 ppm (Figure 5A, cross-signals e). The latter resonance is in turn correlated to the one at 10.9 ppm (Figure 4, cross-peak f), which is also connected to the feature at 13.7 ppm (Figure 4, cross-peak e). We have then identified a four proton network. The location of the ^{13}C NMR signal arising from the carbon attached to the proton at 26.1 ppm (Figure 6, cross-signal t) suggests that this is an anomeric carbon, since it exhibits a larger chemical shift when compared with the other carbon atoms in this network (Figure 6, cross-peaks h−j). On the basis of this evidence, the NMR signals contained in the identified network must arise from a sugar spin subsystem of the type C1H−C2H−C3H−C4H (^1H NMR signals at 26.1, 12.8, 10.9, and 13.7 ppm). Though a chemical shift of 128 ppm is larger than the chemical shifts displayed by the C1 sugar carbons in diamagnetic metallo−BLM derivatives (usually found between 80 and 90 ppm (*17*, *46*)), the large chemical shift difference could be caused by the paramagnetic influence of the Co(II) ion. Since the aromatic carbons in the BLM molecule display chemical shifts between 172 and 114 ppm (*17*, *46*), the sugar C1 carbon signal just discussed would be a good candidate for assignment to an aromatic carbon. However, the fact that this C1 carbon participates in a network of COSY−TOCSY−HMQC connections discards this possibility. As will be discussed later, the two networks of signals identified so far belong to the same sugar moiety, gulose. We have thus been able to assign all the NMR signals generated by this segment.

A third set of COSY-connected signals is detected between 3 and −30 ppm. The COSY spectrum in Figure 5A shows correlations between the signals at −29.9 and −3.0 ppm (cross-peak f) and between the signals at −3.0 and 2.5 ppm (Figure 4, cross-peak h). The latter two are correlated to separate ^{13}C signals in the HMQC spectrum in Figure 6 (cross-peaks o and p). The short T_1 of the −29.9 ppm resonance precludes observation of the ^{13}C signal associated

with it. This network of through bond connections implicates a CH−CH−CH spin subsystem. Besides the spin systems of this type found in the VAL residue, whose NMR signals have already been identified (vide supra), the only residues in the BLM molecule that can give rise to such a network of signals are the sugars.

A fourth network consists of a pair of COSY connected ^{1}H peaks at 3.2 and 2.2 ppm (Figure 3, cross-peak f), which are both connected to the same ^{13}C NMR signal in the HMQC spectrum acquired in D_2O (Figure 6, cross-peak m and n); these observations identify these signals as those arising from another $C6H_2$ group of a sugar fragment.

Up to this point, eleven of the fourteen ^{1}H ^{13}C pairs (including the two CH_2 groups) present in the sugar moieties have been identified through the TOCSY, COSY, and/or HMQC connections they exhibit, but there are still three 1H−13C pairs that need to be tagged. One pair is unobservable, because of the short T_1 of the −29.9 ppm ^{1}H signal. Shown in Figure 6 is a cross-peak (q) whose ^{1}H NMR signal (∼4.8 ppm) is masked by the HDO resonance. The ^{13}C chemical shift corresponding to this cross-feature (92.6 ppm) is consistent with that expected for an anomeric sugar carbon. The last pair is probably the yet unassigned signal at −9.3 ppm (Figure 2B) and its associated ^{13}C whose shift is in the "sugar region" (Figure 6, cross-peak g). Considering that the ^{13}C and ^{1}H NMR signals arising from the nuclei in the GUL segment have already been associated with the two first networks of signals (vide supra), all the other sugar features must come from the nuclei in the MAN segment. From this group of 1H resonances, the ones at 4.8, 3.2, and 2.2 ppm can easily be assigned to the MAN C1H and $C6H_2$ protons. We tentatively assign the CH−CH−CH network to the MAN C3H, C4H, and C5H protons (signals at −29.9, 2.5, and −3.3 ppm, respectively). In the solution structure deduced for HOO−Co(III)BLM (*31*), the MAN C3H is the closest to the metal center of all the mannose protons. The closeness to the metal ion of the MAN C3H proton in Co(II)BLM would account for its short T_1 (*30*). With these assignments in hand, the −9.3 ppm signal is attributed to the MAN C2H proton by elimination.

NMR Signals of the Protons Close to the Metal Ligation Site. At this point, all the ^{1}H (and most of the ^{13}C) signals arising from the nonmetal-coordinated moieties, and the sugars in Co(II)BLM, have been identified (vide supra). Yet unassigned are the NMR features derived from the nuclei in close proximity to the metal including the ALA, PYR, and HIS fragments (*30*, *31*). Unfortunately, many of these resonances are not correlated to other signals and, unlike Fe(II)BLM, cannot be related to their diamagnetic counterparts by ST experiments, thereby making the assignments of the remaining resonances difficult. However, some of them can be attributed to nuclei in the metal-binding region of the molecule by comparison to the assignments for Fe(II)-BLM (*30*). As found for Fe(II)BLM, there are six signals in the NMR spectrum of Co(II)BLM exhibiting some of the largest chemical shifts and shortest relaxation times. These features are located at 211, 152, 114, 77.1, −20.5, and −30.5 ppm, with their T_1 range between 1.0 and 3.7 ms (Table 1). The very strong paramagnetic character of these signals hampers the possibility of finding correlations among them and/or to other features in two-dimensional NMR experiments. Therefore, their one-to-one assignment is not possible at this point. However, these six signals can be attributed to the PYR C$^\beta$H, ALA C$^\beta$H$_2$, ALA C$^\alpha$H, and HIS C$^\alpha$H and C2H protons, assuming a metal coordination environment that involves the HIS amide and imidazole, the pyrimidine, and the ALA amino groups as found for HOO−Co(III)BLM and deduced for Fe(II)BLM (*30*). As in the case of Fe(II)-BLM, the appearance of the six broad signals referred to above, strongly supports the coordination to the metal center of the ALA primary amine. If this group were not bound to the Co(II) center, only five of the broad signals (the ones corresponding to PYR C$^\beta$H, ALA C$^\beta$H$_2$, and HIS C$^\alpha$H and C2H protons) should be detected. In support of the coordination of the ALA primary amine and as observed for Fe(II)-BLM, only one of the two $CONH_2$ pairs of solvent-exchangeable NH protons is observed for Co(II)BLM (Figure 4, cross-peak i). If the ALA primary amine were uncoordinated, then the amide protons in both the PYR and ALA moieties would be six bonds away from the metal center. This should result in the detection of two sets of paired exchangeable resonances for the two $CONH_2$ groups in these moieties, which should be related by COSY peaks. The fact that only one set of COSY-connected solvent-exchangeable resonances is observed in Figure 4 is consistent with the ligation to the metal of the primary amine in ALA. The close proximity of the ALA $CONH_2$ protons to the metal center renders their NMR signals undetectable, so only the PYR $CONH_2$ protons can give rise to the solvent-exchangeable pair of signals observed in Figure 4.

With these assignments, the remaining unidentified protons are on the PYR and HIS segments. The COSY spectrum in Figure 5 shows a connection between the signals at 48.8 and 24.7 ppm (cross-peak c). This COSY connection evidences the presence of either a CH−CH or a CH_2 spin subsystem. Unfortunately, HMQC data that could help discriminate between the two possibilities is not available due to the fast relaxing properties of the 48.8 and 24.7 ppm protons. Nevertheless, the assignments previously made for some of the protons in the ALA−PYR−HIS segment immediately excludes the first option. This is due to either the lack of two vicinal protons with chemical shifts between 50 and 20 ppm or to the large difference in chemical shifts between the assigned and unassigned signals in this segment of the molecule. These facts leave only the CH_2 alternative available, suggesting that the 48.8 and 24.7 ppm signals are derived from the PYR C$^\alpha$H$_2$ group. This result is consistent with their being located three bonds away from a Co(II) coordination site (*47*−*49*). The 48.8 and 24.7 ppm signals exhibit no further correlations to other features in the NMR spectrum of Co(II)BLM.

The previous identification of the methyl groups in THR and VAL (−1.9, −3.4, and −4.9 ppm (vide supra) leaves the signal located at 2.6 ppm (Figure 2D) as the only unassigned methyl signal, which is thus attributed to the PYR CH_3 group. The lack of two-dimensional NMR connections to this feature supports its assignment to the PYR CH_3 group. The coordination to the Co(II) center by the N5 nitrogen in the pyrimidine ring produces only a minor change in the chemical shift of this methyl group (2.0 ppm in apobleomycin (*45*), 2.6 ppm in Co(II)BLM (Table 1)). This situation has also been encountered for Fe(II)BLM (*30*) where the PYR CH_3 group NMR signal is located at 2.1 ppm.

At this point, only signals derived from the protons in the HIS residue are left to be identified. The NMR features arising from the protons in this moiety are difficult to assign due to the lack of COSY and/or TOCSY correlations to any other feature in this segment. Among the ^{1}H NMR features engendered by the HIS protons, the one generated by the aromatic N3H proton can be positively identified at 51.8 ppm (Figure 4B). In the case of coordination to a high spin Co(II) ion by the N1 nitrogen of an imidazole ring, the N3H proton is expected to exhibit an NMR signal between 35 and 70 ppm (*41*, *50*, *51*). In our investigation of the coordination chemistry of Fe(II)BLM (*30*), the C4H proton in the imidazole ring was identified mainly through the connection between the paramagnetic (Fe(II)BLM) and diamagnetic (apo-BLM) versions of the signal in the ST experiments (*30*). Such an experiment was also attempted on Co(II)BLM with no success, which makes difficult the identification of the NMR signal generated by this proton. The NMR data obtained from Co(II)-substituted proteins (*41*) indicate that the signals for C4H protons of N1 Co(II)-coordinated imidazole rings are often found in the region between 40 and 70 ppm. On the basis of these data, the signal positioned at 42.1 ppm in the NMR spectrum of Co(II)BLM (Figure 2B) is assigned to the imidazole C4H proton. The signal at 31.5 ppm is attributed to the HIS C$^\beta$H proton by elimination, having identified all the signals generated by the protons closest to metal. In our NMR study of Fe(II)BLM, the HIS C$^\beta$H proton was found at −17.3 ppm with a relaxation time of 3.1 ms. When compared with each other in a one-to-one fashion, the NMR features engendered by the protons in the Co(II) adduct show relaxation times about two times longer than the ones in the ferrous complex. This comparison supports the assignment of the 31.5 ppm signal to the HIS C$^\beta$H proton. NMR studies performed on Co(II)-substituted proteins, such as azurin (*47*), carboxypeptidase A (*48*), and the liver alcohol dehydrogenase (*49*), indicate that the chemical shift and relaxation time of the 31.5 ppm signal have the right values for a proton located three bonds away from a Co(II) coordination site.

We have thus identified the NMR signals arising from the protons closest to the metal ion in Co(II)BLM. This has been accomplished by taking advantage of the similarities found among the NMR spectra obtained from this BLM adduct and those derived from Fe(II)BLM (*30*), and based on the hypothesis of a common set of ligands for both metallo−BLMs.

The NMR data discussed above allow us to identify some of the ligands to the metal center in Co(II)BLM. Four of them, the N1 and N5 nitrogens in the imidazole and pyrimidine rings, respectively, the secondary amine in ALA, and the amide nitrogen in HIS, have previously been proposed to participate as equatorial ligands to the metal centers for various metallo−BLMs. Comparison of the present NMR results with the ones obtained for Fe(II)BLM (*30*), allowed us to identify the signals generated by the ALA C$^\beta$H$_2$ and C$^\alpha$H protons among the six features exhibiting some of the largest chemical shifts and shortest relaxation times (vide supra). The behavior of these protons indicates that the primary amine on ALA must be an axial ligand.

Given the paramagnetic behavior displayed by most of the sugar protons in the Fe(II)- and Co(II)BLM adducts, the coordination of the mannose to the metal center cannot be ruled out based only on the NMR results. For some of the diamagnetic metallo−BLMs studied so far, the upfield shift exhibited by the mannose C3H proton in the metal bound form, as compared with the apo form, has been considered as evidence that supports the coordination of this sugar to the corresponding metal ion. In the cases of Fe(II)- and Co(II)BLM studied in our lab, the MAN C3H proton exhibits the shortest relaxation time among all the sugar protons. This result, added to the large chemical shifts and short relaxation times of the MAN and GUL protons, could be used to support the coordination of the mannose to the metal center in Co(II)BLM. As discussed above, the NMR data obtained in the present study suggest the binding of the ALA primary amine to the metal center in Co(II)BLM. If both the primary amine and the carbamoyl group were ligands to the metal, then a six-coordinate structure with only endogenous ligands would result for Co(II)BLM. This possibility is examined through molecular modeling in the next section.

MOLECULAR MODELING RESULTS

The aim of this NMR-based structural study is to find the configuration of the Co(II)BLM molecule that is compatible with the NMR data we have generated for it. To this end, we used the four structures for HOO−Co(III)BLM examined by Wu et al. (*31*) to derive 15 alternative starting models, including five- and six-coordinate structures. From the assayed Co(II)BLM models, we shall discuss only the best ones: models I−V, Figure 7. In all models, the metal center was changed from Co(III) to Co(II), and the hydroperoxide ligand was substituted with either the carbamoyl oxygen or a solvent molecule. In all the models considered, the equatorial ligands (secondary amine in ALA, pyrimidine and imidazole rings, and the HIS amide nitrogen) were left unchanged defining what we call the equatorial plane of the metal. Models I and IV involve only endogenous ligands, with the primary amine and the carbamoyl oxygen occupying the axial positions. In these two models, the metal centers have opposite chiralities. Models II and V were derived from models I and IV, respectively, by releasing the carbamoyl oxygen from coordination and substituting it with a solvent molecule. Model III displays the same chirality as model V. However, in the former, the sugar moiety is located on the face of the equatorial plane that is opposite to the one occupied by the bithiazole tail. In the latter, both the sugar residues and the bithiazole tail share the same face of the equatorial plane.

Models I, II, IV, and V were tested based on a spectroscopic investigation of the metal ligation of the ferrous active site of BLM performed by Loeb et al. (*42*). From their studies, they concluded that the spectroscopy is consistent with a six-coordinate, distorted octahedral geometry at the Fe(II) center in Fe(II)BLM. The pyrimidine, imidazole, deprotonated amide, and secondary and primary amine ligands are bound in a pseudo-square pyramidal geometry with either the 3-O-carbamoyl substituent of the MAN or a solvent molecule occupying the sixth site trans to the primary amine. Additionally, the chirality of the metal center and the arrangement of the BLM residues around it, displayed by model II, are similar to those exhibited by structure B for HOO−Co(III)BLM, one of the two possible structures (A and B) proposed by Xu and co-workers (*25*) for this BLM

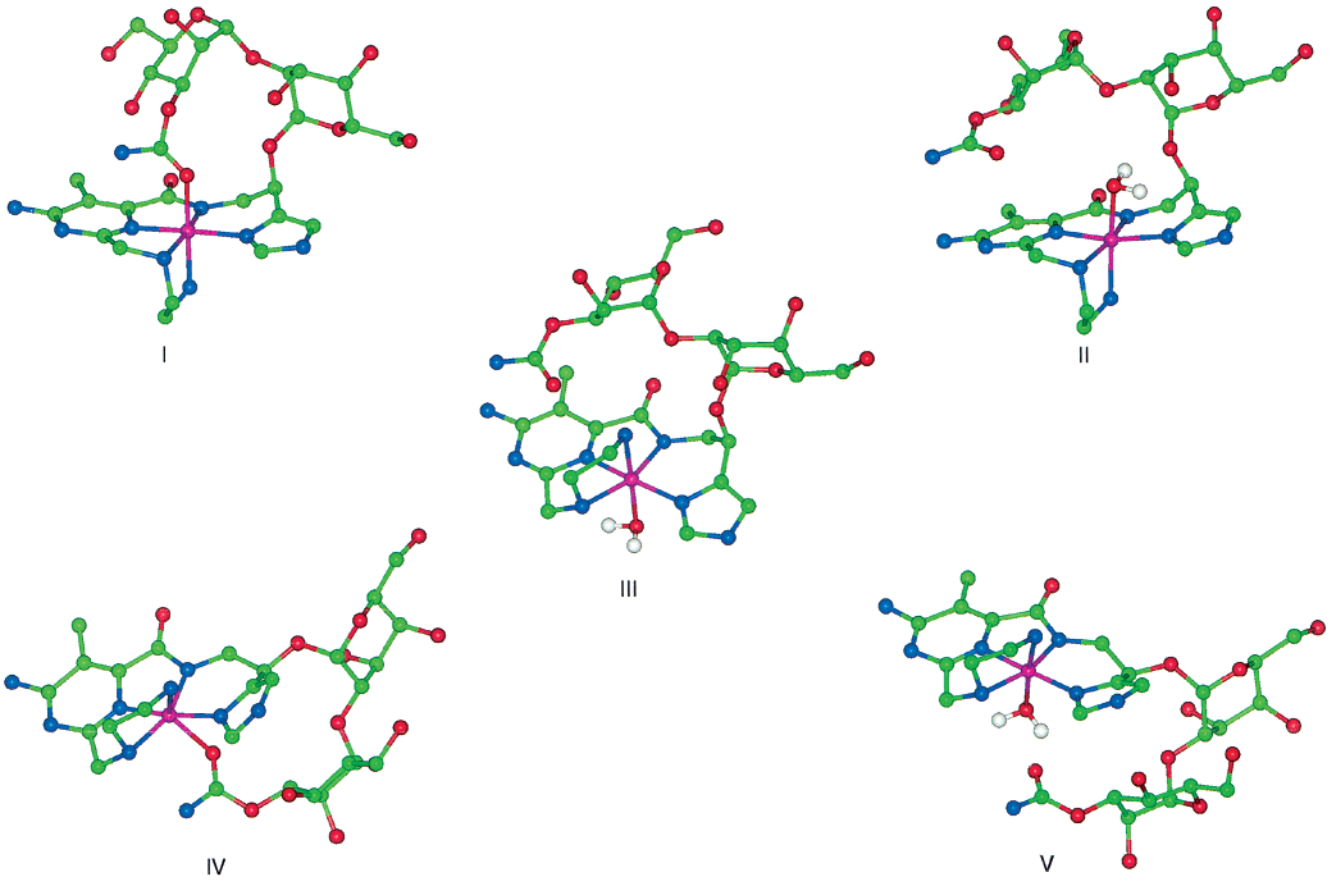

FIGURE 7: Simplified diagrams of the eight models assayed to study the coordination chemistry of Co(II)BLM. The hydrogen atoms have been omitted for simplicity.

adduct in their NMR studies on HOO−Co(III)BLM and Co(III)BLM. Models II and V represent the possibility that the mannose moiety is not bound to the metal center, but just close to it in Co(II)BLM. In this case, the paramagnetic NMR shifts exhibited by the uncoordinated residue would be attributed only to dipolar interactions of this segment with the metal center. Model III could also fulfill the same requirements as models II and V, regarding the paramagnetic behavior of the sugars. This coordination geometry, as well as the arrangement of the unbound BLM fragments around the metal center, has been proposed by Wu et al. (structure I) (*31*) and Xu et al. (structure A) (*25*) for the HOO−Co(III)BLM adduct.

As done for Fe(II)BLM (*30*), proton−metal distances (Hi-Co(II)) were calculated for the protons exhibiting paramagnetic behavior through eq 1 (*52*, *53*). The proton−metal distance for the C4H proton in the imidazole ring was used as the reference value for the calculations, since the imidazole ring is rigid, and when bound to Fe(II) (*54*−*56*) and Co(II) (*57*−*61*), its C4H proton typically displays proton−metal distances of ∼5 Å (Table 1). The distances derived from these calculations were used as constraints for the MD calculations as described in the Materials and Methods section.

The molecular modeling study performed on Co(II)BLM has enabled us to distinguish the NMR signals arising from the two sugars found in the BLM molecule. Since the mannose and gulose moieties present identical spin systems, and due to the lack of a full network of connectivities among the protons belonging to each of these spin systems, it is difficult to decide with which sugar they are associated. Therefore, the examined coordination alternatives were assayed with an assignment of the sugar protons opposite to the one shown in Table 1. The structures derived this way afforded higher total potential and constraint energy values than the corresponding ones obtained with the sugar assignment displayed in Table 1. Therefore, the assignments of the signals to protons on the sugar residues as listed in Table 1 were made based on the quality of the structures obtained.

The results of the molecular modeling are shown in Table 2. The five models we have examined can be separated into two groups: those with five endogenous ligands and a solvent molecule (models II, III, and V; group I), and those with only endogenous ligands (models I and IV; group II). The selection of the configuration of the Co(II)BLM molecule that best fits the experimental data in each group will be guided by the examination of the following parameters (Table 2): rmsd from distance constraints, the geometry of the structure (reflected by the axial angle), the fit of the NMR data vs the structural data (proton−metal distances) to a straight line, constraint energy, and total potential energy. Starting with the models in group I, the comparison of the parameters referred to above between models II and V indicated that the former exhibits a structure that is more compatible with the experimental data than that shown by the latter. Even though both models have very similar total potential energies, model V exhibits higher constraint energy and rmsd from distance constraint values than model II. These results indicate that model V demands more energy to satisfy the constraint requirements, and that the proton−

Table 2: Energy Statistics from Molecular Dynamics

	model I[a]	model II[a]	model III[a]	model IV[a]	model V[a]
potential energy terms[b]					
total	−128.7 ± 1.2	−207.1 ± 1.1	−91.6 ± 1.8	−157.4 ± 1.0	−206.8 ± 2.4
bond	117.3 ± 0.2	118.5 ± 0.1	162.7 ± 0.1	100.7 ± 0.1	102.6 ± 0.3
angle	292.4 ± 0.3	302.4 ± 0.6	416.7 ± 1.8	310.0 ± 0.4	286.2 ± 0.9
torsion	44.2 ± 0.2	22.4 ± 0.3	22.2 ± 0.7	46.8 ± 1.0	42.3 ± 0.7
out-of-plane	1.31 ± 0.03	1.01 ± 0.03	0.59 ± 0.04	2.37 ± 1.1	2.53 ± 0.5
van der Waals	−23.3 ± 1.2	−32.9 ± 0.3	−41.8 ± 0.5	−5.2 ± 0.9	28.0 ± 4.3
electrostatic	−560.8 ± 1.2	−615.1 ± 1.6	−652.4 ± 4.5	−613.1 ± 1.1	−639.8 ± 4.7
constraint	0.17 ± 0.01	0.26 ± 0.01	0.39 ± 0.01	1.00 ± 0.01	1.30 ± 0.1
atomic rmsd for all atoms	0.16 ± 0.06	0.23 ± 0.02	0.24 ± 0.07	0.23 ± 0.05	0.33 ± 0.06
rmsd from distance constraints[c]	0.7	0.7	0.8	1.1	1.2
axial angle[d]	177.8 ± 0.2	174.2 ± 0.2	170.6 ± 0.2	123.1 ± 1.2	172.1 ± 0.9
fits[e]	0.91	0.90	0.94	0.79	0.78

[a] Values derived from the averages of the values obtained for the ten structures generated for each one of the models assayed. [b] Energy terms in kcal mol^{-1}. [c] Calculated with the formula: $\{[\sum(D_{NMR} - D_{Model})^2]/N\}^{1/2}$ where D_{NMR} and D_{Model} are the proton−metal distances derived from the NMR data and the model, respectively, and N is the number of data points. [d] It is the angle among the primary amine, the metal ion, and the carbamoyl oxygen/solvent molecule. [e] Correlation coefficients obtained from the linear fittings of the proton−metal distances derived from the NMR measurements, and the ones obtained from the corresponding model.

metal distances derived from it correlate poorly with the NMR data.

A comparison of models II and III reveals that, except for the total potential energy values being higher for model III, the parameters for the former are only slightly better than those for the latter. The reason for that is the fact that in both models II and III, the mannose and the bithiazole tail are located on different faces of the equatorial plane of the metal. This arrangement seems to satisfy our experimental data better than that exhibited by models IV and V where the sugars and the bithiazole moiety share the same face of the equatorial plane (Table 2). As a matter of fact, as stated at the beginning of this section in the present study, we assessed many starting Co(II)BLM models, including five-coordinate patterns and those where the primary amine is not coordinated. For all the models assayed, regardless of their screw senses, the analysis of the MD results indicated that the patterns with the sugars and the bithiazole tail located on opposite faces of the equatorial plane were better, with respect to the examined parameters, relative to those where these moieties share the same face. Even though the differences between models II and III for four out of the five parameters used to compare the examined patterns are slight, they favor the former over the latter. Additionally, model II has a total potential energy lower than that for model III. On the basis of these results, model II is the one that best fits the experimental data from those in group I.

Group II contains only models I and IV. As can be seen in Table 2, model IV is of lower energy than model I. However, the values of the other four parameters favor model I over model IV. In particular, the axial angle of 123° exhibited by model IV is very distorted from an ideal octahedral structure. Furthermore, the measured proton−metal distances for the MAN C3H and HIS C$^{\beta}$H (3.9 and 3.6 Å, respectively) are shorter than those calculated through the relaxation times (4.3 and 4.4 Å, respectively). If the MAN C3H and HIS C$^{\beta}$H proton−metal distances predicted by model IV were the ones held in solution in the Co(II)BLM molecule, NMR signals with stronger paramagnetic character should be present for these protons in the NMR spectrum. This is not the case as discussed previously. All these facts prompted us to favor model I over model IV in group II.

At this point, the analysis of the MD results (Table 2) has allowed us to select models I and II as the ones that best fit the experimental data we have obtained for Co(II)BLM. Pictures of the full Co(II)BLM molecule for these models are shown in Figure 8. In the discussion that follows, arguments will be made on the basis of the previous structural studies of other metallo−BLMs, to favor model I over model II as the most adequate solution structure for the resting state of CoBLM.

In the structural studies carried out on HOO−Co(III)BLM by Wu et al. (*31*), four coordination alternatives for HOO−Co(III)BLM were examined (structures I−IV). From these alternatives, structures III and IV (primary amine and carbamoyl nitrogen coordinated, respectively, and the same screw sense as our model II) were easily discarded based on their NMR data. However, it was difficult to structurally differentiate between their structures I and II. In fact, they stated that in these two structures both the primary amine and carbamoyl group can be interchanged as axial ligands, with relatively minor structural reorganization. In the final analysis, however, Wu et al. favored structure I as the one held in solution by HOO−Co(III)BLM (*31*). A similar structure was also favored by Xu et al. (structure A) (*25*).

In contrast, the NMR studies performed by Caceres-Cortes et al. (*21*) on HOO−Co(III)PEP led to the proposal of a different structure for this complex where the mannose moiety and the hydroperoxide ligand occupy the axial positions, with the same equatorial ligands as the ones considered in the present study. The structure proposed by Caceres-Cortes and co-workers for HOO−Co(III)PEP (*21*) is similar to Wu's structure II. The complete resonance assignment as well as the determination of the exchange rates of the exchangeable protons in the HOO−Co(III) derivatives of PEP, CoPEP, and CodPEP (*21*), which was not achieved in Wu's study of HOO−Co(III)BLM (*31*), allowed Caceres-Cortes and co-workers to establish that, when present in the PEP molecule, the mannose moiety is coordinated to the metal center instead of the primary amine. These results are also consistent with the findings of Akkermann et al. (*27*) for CO−Fe(II)BLM−A_2 where the mannose NH_2 group is ligated to the iron ion. If the HOO−Co(III)BLM presents a coordination environment similar to the one proposed for

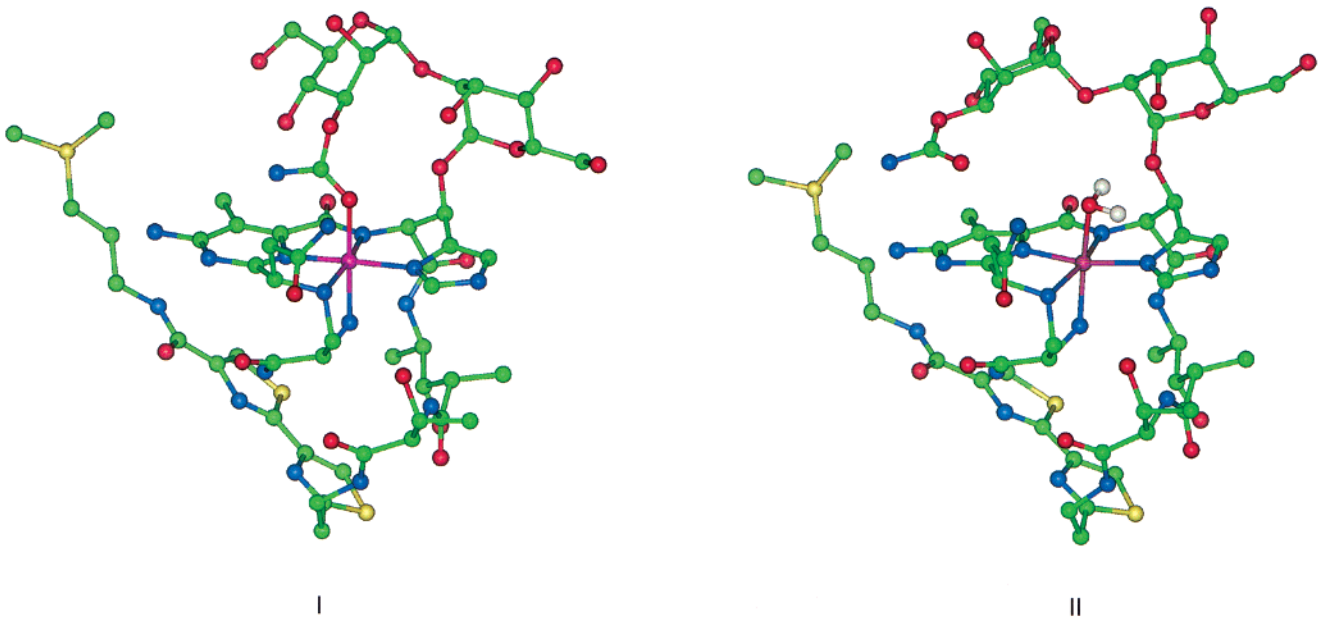

FIGURE 8: Schematic representation of models I and II. These models are the ones that best fit the experimental data. The hydrogen atoms have been omitted for simplicity.

HOO−Co(III)PEP and CO−Fe(II)BLM, then the coordination geometry exhibited by our model I is reasonable for the resting state of this metallo−BLM.

Since Co(II)BLM is the precursor to Co(III)BLM−OOH, the structure of the former should be related to the latter, preferably by a simple ligand substitution process. Such a correlation should be an important factor to consider in assessing our various models. Assuming minimal conformational changes, the Co(III)BLM−OOH structure favored by Wu (structure I) and Xu (structure A) with an axial primary amine ligand can only arise from our model III by displacement of the axial solvent ligand. However, this is a structure already discarded by our NMR data and MD analysis. On the other hand, the structure favored by Caceres-Cortes (axial mannose carbamoyl ligand) can be attained by displacement of the amine ligand from our model I. Co(II)-BLM model I can also give rise to Co(III)BLM−OOH with Wu's structure II and Xu's structure B, both of which were less favored by the respective authors. Model I also displays the same arrangement as the crystallographically characterized Cu(II) complex of P−3A, a biosynthetic precursor of BLM which lacks both the sugar residues and the bithiazole tail present in the BLM molecule. While the absence of the latter residues raises concerns about the validity of Cu(II)P3A as an accurate model for metallo−BLMs, spectroscopic studies performed by Takita et al. (*63*) on Cu(II)BLM suggest that the MAN moiety binds to the Cu(II) center through the carbamoyl oxygen in Cu(II)BLM, affording a structure for the Cu(II) complex that exhibits the exact same coordination geometry as the one displayed by model I. Since model II cannot be easily converted to a Co(II)BLM−OOH structure that is favored by any of the previous investigations, it would seem unlikely to be the structure of the precursor complex. Thus a consideration of all the available data leads us to favor model I, where the Co(II) center is coordinated to all six potential ligating groups of BLM.

Regarding the disposition of the residues in the peptide linker region joining the metal-binding and DNA-binding domains, the slight paramagnetic behavior of the VAL and some of the THR protons indicate that those segments are close to the Co(II) center in Co(II)BLM. The closeness of the peptide linker to the metal center in Co(II)BLM is compatible with the location of this BLM segment suggested by Caceres-Cortes et al. (*21*) and Wu et al. (*31*) for HOO−Co(III)PEP and HOO−Co(III)BLM, respectively. For both HOO−Co(III) complexes, the bithiazole moiety is folded back underneath the equatorial plane of the metal. This location of the BLM tail would bring the VAL−THR segment close to the metal ion, generating the paramagnetic behavior of the protons held by those residues in the Co(II) adduct.

During the NMR studies performed by us on the Fe(II) derivative of BLM (*30*), a structural correlation was established between the NMR data on Fe(II)BLM (H_i−Fe(II) distances) and structures I and II for HOO−Co(III)BLM examined by Wu and co-workers (*31*). Those structures exhibit both the ALA primary amine and the sugar moieties located on the same face of the equatorial plane of the metal. On the basis of these structural correlations, it was proposed that Fe(II)BLM had an arrangement of residues around the metal center similar to the one displayed by Wu's structure I. In the present study, models analogous to Wu's structures I and II were considered. The molecular modeling results for one of them (model III, analogue to structure I) are shown in Table 2. The results for the model analogue to structure II (data not shown) give values of −3.2 and 0.5 kcal $mol,^{-1}$ 1.0, and 0.8 for the total potential and constraint energies, rmsd, and fit of the data, respectively. This model was not included in the discussion, since the primary amine is uncoordinated to Co(II), which is not compatible with our NMR results. If only these two models were considered in the present study, then the conclusion reached for Fe(II)-BLM would still hold for Co(II)BLM. The consideration of all possible coordination geometries compatible with the NMR results has led to a more complete structural study of this metallo−BLM. Molecular modeling of the Fe(II) adduct

of BLM is underway in our lab to establish the arrangement of the drug's residues around this metal center and to determine if, in the resting state, Fe− and CoBLM are isostructural.

CONCLUSIONS

From their studies on Fe(II)BLM, Loeb et al. (*42*) have concluded that this BLM adduct is six-coordinate with at least five endogenous ligands, and either the carbamoyl oxygen or a solvent molecule as the sixth ligand. We have performed structural studies on Co(II)BLM, using the proton−metal distances derived from the relaxation times of the protons close to the metal center as distance constraints. Our molecular modeling calculations indicate that the coordination environment of the metal ion in Co(II)BLM is similar to the one suggested by Loeb and co-workers for Fe(II)BLM (*42*). Additionally, a residue arrangement where the coordinated primary amine is located on the same face as the bithiazole tail and the mannose moiety is located on the opposite face is proposed, based on the comparison of various coordination alternatives examined in the present study. Analysis of some of the most reasonable structures, likely held in solution by some metallo−BLMs, examined in previous structural studies for HOO−Co(II)BLM (*25*, *31*), HOO−Co(III)PEP (*21*), CO−Fe(II)BLM (*27*), and Cu(II)-BLM (*63*) prompted us to proposed a six-coordinate structure with only endogenous ligands for Co(II)BLM.

ACKNOWLEDGMENT

We thank Drs. A. J. Razel and S. J. Lucania of Bristol-Myers Squibb for generously providing us with blenoxane. We are grateful to Dr. Tina Yeh (Scientific Support, Molecular Simulations Inc.) and Dr. Alexander Tropsha (University of North Carolina at Chapel Hill, Medicinal Chemistry and Natural Products) for the invaluable recommendations and comments on the molecular modeling calculations. We are also grateful to Professor JoAnne Stubbe, and Drs. Wei Wu and Dana Vanderwall (Massachusetts Institute of Technology) for sharing with us their structural data on HOO−Co(III)BLM, and for very useful discussions. Our gratitude also goes to Drs. José Domingo Medina (Instituto Venezolano de Investigaciones Científicas (IVIC), Caracas, Venezuela) and Vladimir Alvarado (PDVSA INTEVEP, Caracas, Venezuela) for timely and helpful suggestions.

REFERENCES

1. Stubbe, J., and Kozarich, J. W. (1987) *Chem. Rev. 87*, 1107−1136.
2. Absalon, M. J., Kozarich, J. W., and Stubbe, J. (1995) *Biochemistry 34*, 2065−2075.
3. Absalon, M. J., Wu, W., Kozarich, J. W., and Stubbe, J. (1995) *Biochemistry 34*, 2076−2086.
4. Quadra, J. C., Jr., Zuber, G. F., and Hecht, S. M. (1998) *Pure Appl. Chem. 70*, 307−311.
5. Fulmer, P., Zhao, C., Li, W., DeRose, E., Antholine, W. E., and Petering, D. H. (1997) *Biochemistry 36*, 4367−4374.
6. Suh, D., and Povirk, F. (1997) *Biochemistry 36*, 4248−4257.
7. Sam, J. W., Takahashi, S., Lippai, I., and Peisach, J. (1998) *J. Biol. Chem. 273*, 16090−16097.
8. Bailly, C., Kénani, A., and Waring, M. J. (1997) *Nucleic Acids Res. 25*, 1516−1522.
9. Bansal, M., Stubbe, J., and Kozarich, J. W. (1997) *Nucleic Acids Res. 25*, 1846−1853.
10. Burger, R. M. (1998) *Chem. Rev. 98*, 1153−1169.
11. Wu, W., Vanderwall, D. E., Turner, C. J., Kozarich, J. W., and Stubbe, J. (1996) *J. Am. Chem. Soc. 118*, 1281−1294.
12. McGall, G. H., Rabow, L. E., Ashley, G. W., Wu, S. H., Kozarich, J. W., and Stubbe, J. (1992) *J. Am. Chem. Soc. 114*, 4967−4975.
13. Dabrowiak, J. C. (1982) *Adv. Inorg. Biochem. 4*, 69−113.
14. Boger, D. L., Ramsey, T. M., Cai, H., Hoehn, S. T., and Stubbe, J. (1998) *J. Am. Chem. Soc. 120*, 9139−9148.
15. Boger, D. L., Ramsey, T. M., Cai, H., Hoehn, S. T., and Stubbe, J. (1998) *J. Am. Chem. Soc. 120*, 9149−9158.
16. Oshitari, T., Shibasaki, M., Yoshizawa, T., Tomita, M., Takao, K.-I., and Kabayashi, S. (1997) *Tetrahedron 32*, 10993−11006.
17. Kimura, E., Kurosaki, H., Kurigi, Y., Shionoya, M., and Shiro, M. (1992) *Inorg. Chem. 31*, 4314−4321.
18. Roelfes, G., Lubben, M., Leppard, S. W., Schudde, E. P., Hermant, R. M., Hage, R., Wilkinson, E. C., Que, L., Jr., and Feringa, B. L. (1997) *J. Mol. Catal. A: Chemical 117*, 223−227.
19. Boger, D. L., Ramsey, T. M., Cai, H., Hoehn, S. T., Kozarich, J. W., and Stubbe, J. (1998) *J. Am. Chem. Soc. 120*, 53−65
20. Ghirlanda, G., Scrimin, P., Tecilla, P., and Toffoletti, A. (1998) *Langmuir 14*, 1646−1655.
21. Caceres-Cortes, J., Sigiyama, H., Saito, I., and Wang, A. H.-J. (1997) *Eur. J. Biochem. 244*, 818−828.
22. Calafat, A. M., Won, H., and Marzilli, L. G. (1997) *J. Am. Chem. Soc. 119*, 3656−3664.
23. Stubbe, J., Kozarich, J. W., Wu, W., and Vanderwall, D. E. (1996) *Acc. Chem. Res. 29*, 322−330.
24. Mandervill, R. A., Ellena, J. F., and Hecht, S. M. (1995) *J. Am. Chem. Soc. 117*, 7891−7903.
25. Xu, R. X., Nettesheim, D., Otvos, J. D., and Petering, D. H. (1994) *Biochemistry 33*, 907−916.
26. Wu, W., Vanderwall, D. E., Stubbe, J., Kozarich, J. W., and Turner, C. J. (1994) *J. Am. Chem. Soc. 116*, 10843−10844.
27. Akkerman, M. A. J., Neijman, E. W. J. F., Wijmenga, S. S., Hilbers, C. W., and Bermel, W. (1990) *J. Am. Chem. Soc. 112*, 7462−7474.
28. Sheridan, R. P., and Gupta, R. K. (1981) *J. Biol. Chem. 256*, 1242−1247.
29. Sheridan, R. P., and Gupta, R. K. (1981) *FEBS Lett. 134*, 226−230.
30. Lehmann, T. E., Ming, L.-J., Rosen, M. E., and Que, L., Jr. (1997) *Biochemistry 36*, 2807−2816.
31. Wu, W., Vanderwall, D. E., Lui, S. M., Tang, X.-J., Turner, C. J., Kozarich, J. W., and Stubbe, J. (1996) *J. Am. Chem. Soc. 118*, 1268−1280.
32. Akkerman, A. J., Haasnoot, C. A. G., Pandit, U. K., and Hilbers, C. W. (1988) *Magn. Reson. Chem. 26*, 793−802.
33. Pillai, R. P., Lenkinski, R. E., Sakai, T. T., Geckle J. M., Krishna, N. R., and Glickson, J. D. (1980) *Biochem. Biophys. Res. Comm. 96*, 341−349.
34. Oppenheimer, N. J., Rodriguez, L. O., and Hecht, S. M. (1979) *Biochemistry 16*, 3439−3445.
35. Xu, R. X., Antholine, W. E., and Petering, D. H. (1992) *J. Biol. Chem. 267*, 944−949.
36. Xu, R. X., Antholine, W. E., and Petering, D. H. (1992) *J. Biol. Chem. 267*, 950−955.
37. Tan, J. D., Hudson, S. E., Brown, S. J., Olmstead, M. M., and Mascharak, P. K. (1992) *J. Am. Chem. Soc. 114*, 3841−3853.
38. Saito., I., Morii, T., Sugiyama, H., Matsura, T., Meares, C. F., and Hecht, S. M. (1989) *J. Am. Chem. Soc. 111*, 2307−2308.
39. Chang, C.-H., and Meares, C. F. (1982) *Biochemistry 21*, 6332−6334.
40. Burger, R. M., Peisach, J., and Horwitz, S. B. (1981) *J. Biol. Chem. 256*, 11636−11644.
41. Bertini, I., Turano, P., and Vila, A. J. (1993) *Chem. Rev. 93*, 2833−2932.

42. Loeb, K. E., Zaleski, J. M., Hess, C. D., Hecht, S. M., and Solomon, E. I. (1998) *J. Am. Chem. Soc. 120*, 1249−1259.
43. Petering, D. H., Byrnes, R. W., and Antholine, W. E. (1990) *Chem.-Biol. Interact. 73*, 133−182.
44. Chen, D. M., Hawkins, B. L., and Glickson, J. D. (1997) *Biochemistry 16*, 2731−2736.
45. Haasnoot, C. A. G., Pandit, U. K., Kurk, C., and Hilbers, C. K. (1984) *J. Biomol. Struct. Dyn. 2*, 449−467.
46. Williamson, D., McLennan, I. J., Bax, A., Gamcsik, M. P., and Glickson, J. D. (1990) *J. Biomol. Struct. Dyn. 8*, 375−398.
47. Salgado, J., Jiménez, H. R., Donaire, A., and Moratal, J. M. (1995) *Eur. J. Biochem. 231*, 358−369.
48. Bertini, I., Canti, G., and Luchinat, C. (1982) *J. Am. Chem. Soc. 104*, 4943−4951.
49. Bertini, I., Gerber, M., Lanini, G., Luchinat, C., Maret, W., Rawer, S., and Zeppezauer, M. (1984) *J. Am. Chem. Soc. 106*, 1826−1830.
50. Bertini, I., Lanini, G., Luchinat, C., Messori, L., Monnanni, R., and Scozzafava, A. (1985) *J. Am Chem. Soc. 107*, 4391−4405.
51. Banci, L., Bertini, I., Luchinat, C., and Sozzafava, A. (1987) *J. Am. Chem. Soc. 109*, 2328−2332.
52. Bertini, I., and Luchinat, C. (1986) in *NMR of Paramagnetic Molecules in Biological Systems* (Lever, A. B. P., and Gray H. B., Eds.) pp 19−45, The Benjamin & Cummings Publishing Company, Inc., Menlo Park, CA.
53. La Mar, G., and de Ropp J. S. (1993) in *NMR of Paramagnetic Molecules* (Berliner, L. J., and Reuben, J., Eds.) pp 1−73, Plenum Press, New York.
54. Tolman, W. B., Shuncheng, L., Bentsen, J. G., and Lippard, S. J. (1991) *J. Am. Chem. Soc. 113*, 152−164.
55. Mandon, D., Ott-Woelfel, F., Fischer, J., Weiss, R., Bill, E., and Trautwein, A. X. (1990) *Inorg. Chem. 29*, 2442−2447.
56. Spek, A. L., Duisenberg, A. J. M., and Feiters, M. C. (1983) *Acta Crystallogr. C 39* 1212−1218.
57. Farinas, E., Baidya, N., and Mascharak, P. K. (1994) *Inorg. Chem. 33*, 5970−59743.
58. Horrocks, W. D., Jr., Ishley, J. N., and Whittle, R. R. (1982) *Inorg. Chem. 21*, 3270−3272.
59. Pattabhi, V., Nethaji, M., Gabe, E. J., Lee, F. L., and Le Page, Y. (1984) *Acta Crystallogr. C 40*, 1155−1158.
60. Horrocks, W. D., Jr., Ishley, J. N., and Whittle, R. R. (1982) *Inorg. Chem. 21*, 3265−3267.
61. Mao, Q., Fulmer, P., Li, W., De Rose, E. F., and Petering, D. H. (1996)*J. Biol. Chem. 271*, 6185−6191.
62. Iitaka, Y., Nakamura, H., Nakatani, T., Muraoka, Y., Fujii, A., Takita, T., and Umezawa, H. (1978) *J. Antibiot. 31*, 1070−1072.
63. Takita, T., Muraoka, Y., Nakatani, T., Fujii, A., Iitaka, Y., and Umezawa, H. (1978) *J. Antibiot. 31*, 1073−1077.

BI991841P